Received August 12, 2019, accepted August 22, 2019, date of publication August 29, 2019, date of current version September 20, 2019.

Digital Object Identifier 10.1109/ACCESS.2019.2938207

Impact of Grid Impedance on LVRT Performance of DFIG System With Rotor Crowbar Technology

ZAKIUD DIN[1], JIANZHONG ZHANG[1], (Senior Member, IEEE), YAODONG ZHU[2], ZHENG XU[1], AND AHMED EL-NAGGAR[3], (Senior Member, IEEE)

[1]School of Electrical Engineering, Southeast University, Nanjing 210096, China
[2]School of Mechanical and Electrical Engineering, Jiaxing University, Jiaxing 314001, China
[3]GE Energy Consulting, 80807 Munich, Germany

Corresponding author: Yaodong Zhu (nuaazyd@mail.zjxu.edu.cn)

This work was supported in part by the National Natural Science Foundation of China under Grant 51577025, and in part by the Zhejiang Key Research and Development Project under Grant 2017C01043.

ABSTRACT Nowadays, most of the doubly fed induction generators (DFIGs) are equipped with rotor crowbar for the requirement of low voltage ride through (LVRT). The crowbar resistance is an important parameter, and it is selected taking rotor overcurrent and dc link overvoltage limits into consideration. However, the impact of grid impedance on the LVRT performance of DFIG and crowbar resistance is not adequately researched. This paper proposed an improved method to analyze the LVRT performance of DFIG system with rotor crowbar taking the influence of the grid impedance to fill this gap. The impedance of the present grid would be decreased in the future due to the installation of more wind farms to the grid. As a consequence, the performance of DFIG under LVRT with rotor crowbar is degraded. So the design rules of the crowbar resistance need to be reconstructed. Additionally, the analytical expression of the crowbar resistance is derived considering the grid impedance. The effectiveness of the proposed method is validated through theoretical analysis and MATLAB simulations.

INDEX TERMS DFIG, crowbar, grid impedance, wind energy, low voltage ride through.

I. INTRODUCTION

In recent years, wind power plays a significant role in the power system due to the high penetration of wind energy into the power grid. The wind energy conversion system should meet the requirements of the grid voltage control, and this is termed as fault ride-through or low voltage ride- through (LVRT) to guarantee the stability of power system in grid faults scenarios. Additionally, the LVRT for wind farm grid code is indispensable. China has been the largest market of wind turbines in the world in recent years, and it is reported that wind energy is 164 Giga-watts by 2017 and is expected to be 210 Giga-watts by 2020. In 2003, the German electric transmission operator E.ON and VE-T firstly defined the LVRT [1], and it has been the research hotspot for more than one decade.

According to grid code of China, wind turbines are required to ride-through voltage dips down to 20% of nominal grid voltage, without tripping offline for the duration of 625 milliseconds, or absorbing reactive power from the power grid as depicted in Fig. 1.

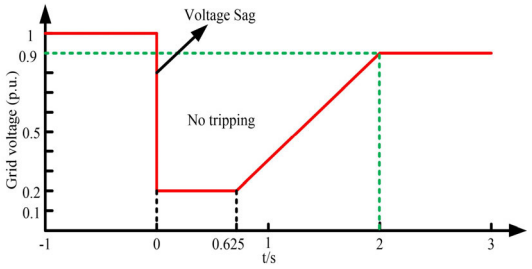

FIGURE 1. LVRT standards of state grid of China.

Advantages like partial rated power converter and variable speed operations make DFIG prevalent in the wind power industry [2]. However, the DFIG system is more vulnerable to grid disturbances due to the direct connection of the stator circuit to the grid. The voltage at PCC is dropped due to the grid faults, resulting in a high stator transient current. The magnetic coupling between stator and rotor circuit causes high voltage and current in the rotor circuit. As a consequence, high current flows through the rotor side converter (RSC), and the RSC faces high electrical stress due to overcurrent and/or overvoltage. Moreover, mechanical stress is also generated on the bearings and gearbox, which worsen the lifespan of the gearbox.

The associate editor coordinating the review of this manuscript and approving it for publication was Zhehan Yi.

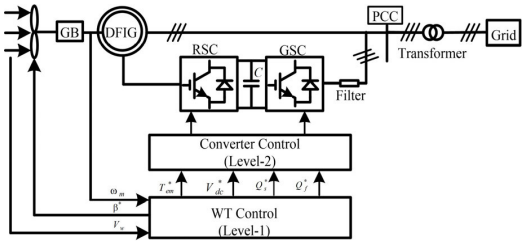

FIGURE 2. Schematic diagram of a DFIG system.

Fig. 2 shows the schematic diagram of the DFIG system. To allow the converter to generate or absorb reactive power [3], the RSC controlled the stator active and reactive power, and the dc-link voltage is controlled by the grid side converter (GSC). However, the wind speed can change the active power flow direction through the rotor circuit [4], [5].

In literature, numerous LVRT techniques have been proposed to improve the LVRT capability of the DFIG system and can be generally divided into types of (i) hardware based solutions [6]–[18] and (ii) software based solutions [18]–[27]. A series coupled compensation converter [6], and a cascade converter [7] are proposed to fulfill the LVRT requirements of a DFIG system. But most of the hardware based protection schemes for a wind turbine in the industry deployed the crowbar to limit the high current and voltage in the rotor circuit [8]–[10]. During grid faults, the crowbar circuit is triggered, and the RSC is blocked to keep the rotor current in prescribed limits. Consequently, DFIG operates like a squirrel cage induction generator absorbing reactive power from the faulty grid [11]. To enhance the performance of the DFIG system under LVRT, some improved crowbar solutions have been proposed [12]–[18]. Nevertheless, the grid impedance is not taken into consideration during the crowbar resistance selection.

Software based solutions such as enhanced hysteresis based current regulators [19], and the modified feed-forward compensating term [20] are usually employed in the vector control structure. Furthermore, in the literature, advanced control methods such as nonlinear control approach [21], power angle control [22] and the adaptive disturbance rejection control [23] are presented to improve the DFIG performance under LVRT. The hybrid fuzzy PI-cascade controller and the coordinated reactive power control to fulfill the LVRT requirements of DFIG system are proposed in [24] and [25], respectively. Reference [26] proposed an inductance-emulating control strategy to enhance the LVRT capability of the DFIG system. Reference [27] proposed the improved rotor braking protection in coordination with self-adaptive control to further improve the LVRT performance of the DFIG system. [28] anticipated novel techniques through peak short circuit current reduction to enhance the LVRT capabilities of the DFIG system. However, part of the above control strategies suffers from complexity and lack of robustness.

Improvement in the LVRT performance of DFIG system using rotor crowbar is the research hotspot for both academia and industry. However, the impact of grid impedance on the crowbar resistance (R_c) is neglected. The future grid will be influenced by connecting more wind farm. Hence the impedance of the future grid will be decreased, and the DFIG performance under LVRT will be deteriorated. So this paper analyzed the impact of grid impedance on the LVRT performance of the DFIG system with rotor crowbar solutions.

This paper is organized as follows. The modeling of a DFIG system is discussed in Section II. Control of DFIG system during steady state and grid voltage dips is briefly discussed in section III. Selection and comparison of the crowbar resistance with different methods and possible modifications in the rotor crowbar to further improve DFIG performance under LVRT support are discussed in section IV. A brief discussion about the modified method and the traditional method of crowbar resistance selection is made in Section V. Finally; conclusions are drawn in section VI.

II. MODELING

The DFIG system includes a wind turbine, drive train model, the generator, back to back power converter together with its control system and connects with the grid through the transformer (See Fig. 2). The control system has two levels. One is the wind turbine (WT) control, and the second is converter control. The WT level generates the reference value for the rotor speed of the DFIG based on the measured wind speed and optimum power-speed characteristic curve. It also controls the output mechanical power of the wind turbine through the pitch angle. The two-level control strategy is used for both power optimization and power limitation below and above the rated speed, respectively [29]. The converter control, i.e., the controllers of RSC and GSC, decouple the active and reactive power and will be briefly introduced in the forthcoming sections of this paper.

A. DRIVEN TRAIN

The whole mechanical system model for a wind turbine is very complex and rigorous calculations are needed. However, for the simulation case in this paper, two mass driven train model is sufficient, as shown in Fig. 3. The turbine rotational speed (Ω_{t_ar}) and torque (τ_{t_ar}) can be expressed as [30]:

$$\Omega_{1\_ar} = N\Omega_1 \tag{1}$$

$$\tau_{1\_ar} = \frac{\tau_{1\_ar}}{N_{gb}} \tag{2}$$

where N_{gb} is the gearbox ratio. The first order differential equation of two mass systems is given by

$$J_1 \frac{d\Omega_{1\_ar}}{dt} = \tau_{1\_ar} - D_1\Omega_{1\_ar} - \tau_{e2} \tag{3}$$

$$J_2 \frac{d\Omega_2}{dt} = \tau_{e2} - D_2\Omega_2 + \tau_{e2} \tag{4}$$

$$\frac{d\tau_{e2}}{dt} = K_{12}(\Omega_{1\_ar} - \Omega_2) + D_{12}\left(\frac{d\Omega_{1\_ar}}{dt} - \frac{d\Omega_2}{dt}\right) \tag{5}$$

The model can be simplified into two inertia (J_1 and J_2) and stiffness (K_{12}) by ignoring the damping coefficients (D_1, D_2, and D_{12}).

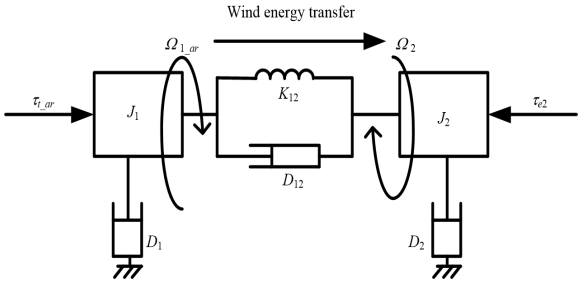

FIGURE 3. Two mass driven train model.

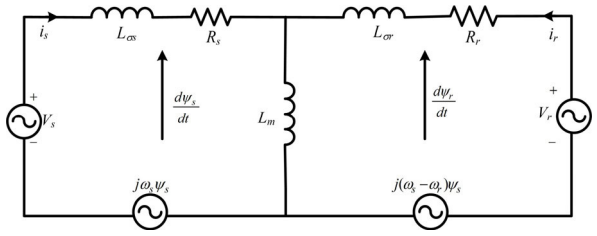

FIGURE 4. Equivalent circuit of DFIG.

B. GENERATOR

The stator voltage and rotor voltage are derived from Fig. 4, where the stator and rotor flux in an arbitrary frame of reference rotating with angular speed ω. According to [30], it has

$$V_s = R_s I_s + \frac{d\psi_s}{dt} + j\omega_s \psi_s \tag{6}$$

$$V_r = R_r I_r + \frac{d\psi_r}{dt} + j(\omega - \omega_s)\psi_r \tag{7}$$

$$\psi_s = L_s I_s + L_m I_r \tag{8}$$

$$\psi_r = L_m I_s + L_r I_r \tag{9}$$

where V_s and V_r are stator and rotor voltage. R_s and R_r are the stator and rotor resistance. ψ_s and ψ_r represent stator and rotor flux linkage. L_s, L_r and L_m is the stator and rotor self and mutual inductance, respectively.

By aligning d-axis reference frame to air gap flux of the DFIG, the electromagnetic torque and reactive power can be expressed as

$$T_e = -\frac{\psi_{sd} \cdot L_m}{L_s} i_{rq} \tag{10}$$

$$Q_s = \frac{\psi_{sd} \cdot \psi_{sd}}{L_{\sigma s}} - \frac{\psi_{sd} \cdot L_m}{L_{\sigma s}} i_{rd} \tag{11}$$

The electromagnetic torque and stator reactive power is directly proportional to q-axis and d-axis rotor current, respectively. RSC controls the electromagnetic torque (or active power) and reactive power by decoupling i_{rd} and i_{rq}.

C. CROWBAR

Crowbar is connected between the rotor of the DFIG and the RSC, as shown in Fig. 5. Thyristor might be used as a switch in crowbar circuit in the early stage of the grid-connected wind turbine system, but thyristor suffers from disadvantages of uncontrollability of their cut-off. Most of the manufacturers replace thyristor with IGBT to allow direct disconnection

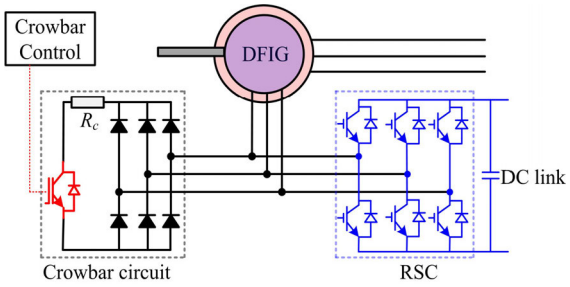

FIGURE 5. Rotor crowbar protection circuit.

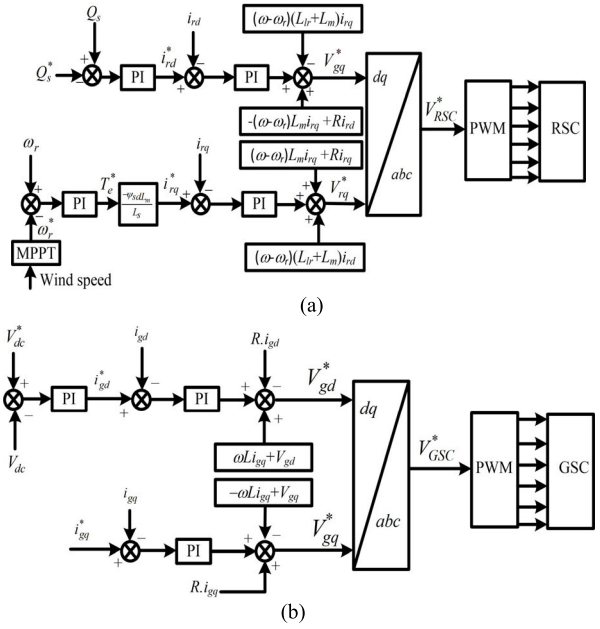

FIGURE 6. Vector control for DFIG. (a) RSC vector control scheme, (b) GSC vector control scheme.

of a crowbar and instant RSC reactivation to resume the normal operation. The IGBTs of the RSC are blocked, and the crowbar is activated, if either the rotor current or the dc-link voltage levels exceed the limits. The voltage across the R_c and dc-link voltage are examined during the crowbar action. The crowbar is disengaged, when both of these voltages are sufficiently low. After a small delay for the decay of the rotor currents, the RSC will be reactivated, and the reactive power is supplied for grid support.

During normal operation, the RSC and GSC are in action, and the crowbar is in OFF mode. The IGBT of the active crowbar must be turned on to bypass the rotor overcurrent from the RSC to crowbar to restrain the rotor overvoltage during voltage dips.

III. CONTROL STRATEGIES

A. VECTOR CONTROL

The vector control of power converters for the DFIG is based on coordinate transformation with the use of the conventional PI controller. Various publications [12], and [32], [33] have been published regarding the vector control of the DFIG. The vector control structure for the DFIG is shown in Fig. 6.

The RSC control structure has the inner current control loop and the outer torque or speed control loop. The electromagnetic torque and reactive power of DFIG are controlled independently by controlling the RSC in synchronously rotating d-q frame of reference aligning d-axis to the stator flux. The reference q-axis rotor current i_{rq}^* is generated by regulating the reference torque T_e^* over the rotor speed. The reference rotor speed ω_r^* is calculated using the maximum power point tracking (MPPT) algorithm. The reference d-axis rotor current i_{rd}^* is generated by regulating the reactive power supplied by the DFIG, as shown in Fig. 6(a).

The goal of the GSC is to retain the constant voltage on the dc link capacitor regardless of the sub and super synchronous mode of operation. In the synchronous frame of reference, the voltage balance equation can be expressed as

$$\begin{cases} v_{gd}^* = Ri_{gd} + L\dfrac{di_{gd}}{dt} - \omega L i_{gq} + v_{gd} \\ v_{gq}^* = Ri_{gq} + L\dfrac{di_{gq}}{dt} - \omega L i_{gd} + v_{gq} \end{cases} \tag{12}$$

By aligning d-axis of the synchronous frame of reference to the grid voltage, the active power supplied and absorbed by the GSC to/from the grid is given by

$$\begin{cases} P = \dfrac{3}{2} v_{gd} i_{gd} \\ Q = \dfrac{3}{2} v_{gd} i_{gq} \end{cases} \tag{13}$$

The control strategy for the GSC is shown in Fig. 6(b). The active power and hence, the dc link voltage is directly proportional to i_{gd}, and reactive power is proportional to i_{gq}, which can be regulated by controlling v_{gd}^* and v_{gq}^*, respectively. By application of a PI controller over dc link voltage v_{dc}, the reference d-axis GSC current i_{gd}^* is calculated, where the q-axis reference GSC current (i_{gq}^*) is set equal to zero. To control the current loops, the reference voltage (V_{GSC}^*) is calculated for GSC by using (12).

B. LVRT CONTROL WITH CROWBAR

From the viewpoint of the converter, the rotor voltage is one of the most critical parameters of the DFIG system during grid voltage dips [13]. The rotor flux linkage can be found by combining (8) and (9) and is given by

$$\vec{\psi}_r = \frac{L_m}{L_s}\vec{\psi}_s - \sigma L_r \vec{i}_r \tag{14}$$

where $\sigma = 1 - L_m^2/(L_s L_r)$ is the leakage coefficient, and σL_r is the transient rotor inductance.

The rotor voltage can be found by substituting (14) into (7) and can be expressed as [15]

$$\vec{v}_r = \frac{L_m}{L_s}\frac{d\vec{\psi}_s}{dt} + (R_r + \sigma L_r \frac{d}{dt})\vec{i}_r \tag{15}$$

As can be seen in (15), the rotor voltage consists of two parts. The first part is the EMF induced in the rotor circuit by stator flux linkage; the voltage drop on both resistance and transient inductance can be treated as a second part.

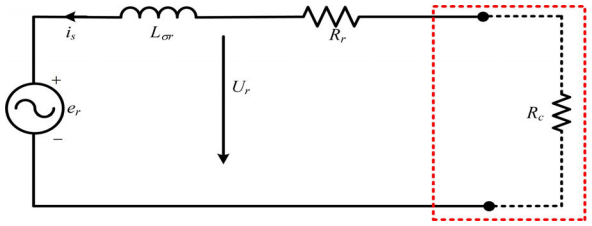

FIGURE 7. Rotor side equivalent circuit of DFIG with a crowbar.

The EMF under steady state, neglecting the stator resistance of the DFIG is given by

$$\vec{e}_r = \frac{L_m}{L_s}\frac{d\vec{\psi}_s}{dt} = \frac{L_m}{L_s} s U_{s0} e^{js\omega_s t} \tag{16}$$

where U_{s0} is the rated stator voltage. It shows the rotor EMF is directly proportional to slip s and the slip range is $+0.3$ to -0.3. So according to (16), under normal grid condition, the rotor EMF will be within $\pm 30\%$ of the rated stator voltage. The stator flux comprises various transient component during symmetrical grid faults scenarios, and the stator flux under such scenarios is given by

$$\vec{\psi}_s = \frac{(1-d)U_{s0}}{j\omega_s} + \frac{dU_{s0}}{j\omega_s} e^{-\frac{t}{\tau_s}} \tag{17}$$

where $\tau_s = L_s/R_s$ and d represents voltage dips depth degree and time constant of the stator flux, respectively.

Based on (16) and (17), the EMF under symmetrical is given by [15]

$$\vec{e}_r = \frac{L_m}{L_s}\left[s(1-d)U_{s0} e^{js\omega_s t} - d(1-s)U_{s0} e^{-j\omega_r t} e^{-t/\tau_s} \right] \tag{18}$$

The first term of (18) is a positive sequence component of rotor EMF, and the rest proportional to $(1 - s)$ is the transient component. Under full voltage dip with $s = -0.3$, the initial amplitude is $1.3 U_{sN} L_m/L_s$, which shows the high initial amplitude of the rotor EMF.

The aforementioned analysis concluded the output voltage of RSC would be increased during grid fault scenarios due to high rotor EMF. In such cases, the rotor crowbar must be activated to bypass the RSC. Fig. 7 shows the rotor side equivalent circuit with a crowbar.

IV. OPTIMIZATION OF CROWBAR RESISTANCE

In this paper, only the crowbar for DFIG system is considered. The crowbar circuit will bypass the RSC to limit the high currents and voltages in the rotor circuit under grid fault scenarios. There are two main requirements which give the upper and lower limit of R_c. To limit the rotor current, R_c should be large enough. However, to elude a too high voltage in the rotor circuit R_c must be small. So the tradeoff should be made between the upper and lower limits of R_c. It should be noted that other control strategies, i.e., direct torque control could also be applied to the DFIG system for realizing the LVRT of the DFIG system and the rotor crowbar will be similar.

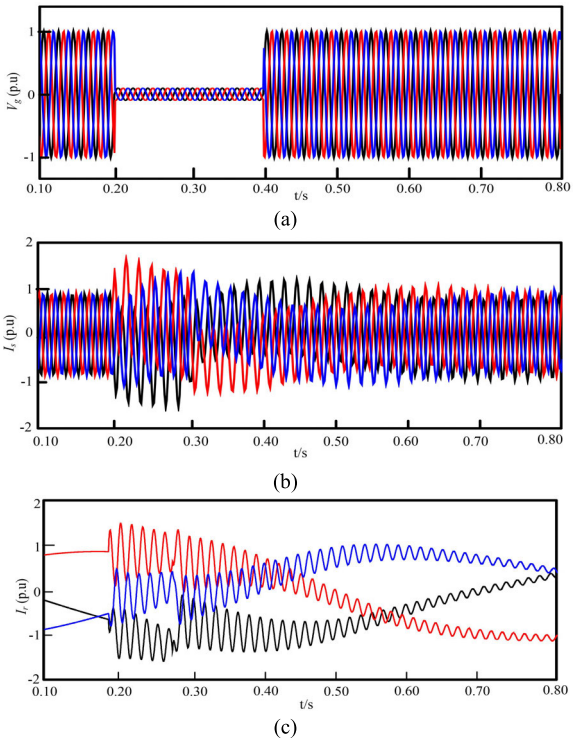

FIGURE 8. Simulation results of method-1 under 90% voltage dip. (a) Grid voltage, (b) Stator current, (c) Rotor current.

A. TRADITIONAL ROTOR CROWBAR RESISTANCE

In [34], the crowbar circuit is tested for different degree of the voltage dips, i.e., 0 %, 15% and 40%, and the optimized R_c is given as

$$R_c = \omega_r \sqrt{L_s L_\sigma - 2L_\sigma^2} \tag{19}$$

where $L_s = L_{\sigma s} + L_m$ and $L_\sigma = L_{\sigma s} + L_{\sigma r}$, $L_{\sigma s}$, and $L_{\sigma r}$ are the self-inductance of stator and rotor windings respectively, and L_m is the mutual inductance. Theoretical results are verified through simulations, but in the proposed configuration, R_c depends on the machines parameters, i.e., inductances and angular frequency of the DFIG. Additionally, the maximum allowable rotor voltage limit is not defined in the proposed method.

Voltage dip or voltage sag is a sudden reduction (between 10% and 90%) of the voltage at a point. In this paper, a little higher voltage dips (90%) than China LVRT standards (80%), and a little lower than Germany (100%), Sweden and Finland (95%) is selected. Additionally, in this paper, the DFIG system with R_c selected by (19) is defined as method-1 and simulated under 90% voltage dip at PCC. Fig. 8 shows the simulation results of the DFIG with parameters of the DFIG system are given in Table 1.

The stator and rotor current is shown in Fig. 8(b) and Fig. 8(c), respectively. It can be seen in Fig. 8(b) that the stator current under 90% voltage dip from 0.2 to 0.4 seconds is under the limit of overcurrent. Similarly, the rotor current

TABLE 1. Simulation parameters of DFIG [31].

Symbol	Value	Symbol	Value
V_s	575 V	R_s	0.023 p.u.
V_r	0.32 p.u.	R_r	0.016 p.u.
f	50 Hz	V_{dc}	1150 V
$L_{\sigma s}$	0.18 p.u.	C_{dc}	80 mF
$L_{\sigma r}$	0.16 p.u.	ω_r	1.2 p.u.
L_m	2.9 p.u.	Pole pairs	2

lies under the safe operating limit, i.e., 2 p.u. as can be seen in Fig. 8(c).

There is another selection way for rotor crowbar resistance given in [35]. By assuming the short-circuit at the generator stator terminal of grid-connected DFIG, R_c can be given as

$$R_c < \frac{\sqrt{2} V_{r\max} X_s'}{\sqrt{3.2 V_s^2 - 2V_{r\max}^2}} \tag{20}$$

where V_{rmax} is the permissible rotor voltage, $X_s^{'}$ is the transient reactance of the rotor windings and V_s is the stator voltage under grid fault.

Maximum rotor voltage is used in [36] to extract R_c and as given by

$$R_c < \frac{\sqrt{2} V_{r\max} X_{\sigma r}}{\sqrt{\frac{L_m^2}{L_s^2}(2-s)^2 V_s^2 - 2V_{r\max}^2}} \tag{21}$$

where V_{rmax} and V_s is the maximum rotor voltage and stator voltage, respectively. L_m, L_s is the mutual and stator steady state inductance respectively, $X_{\sigma r}$ is the transient reactance of the rotor windings. It can be seen from (20) and (21) that the expression of R_c is nearly the same, considering the maximum allowable rotor voltage, stator voltage and transient inductance. However, author [36] gives more theoretical and mathematical analysis to find the exact and more practical value of R_c as compared to [35], where too many assumptions and rough approximation are taken into consideration. The DFIG with R_c selected by (21) will be treated as method-2 in this paper to simplify the analysis.

The simulation results of stator and rotor currents with the crowbar circuit (method-2) are shown in Fig. 9, where 90% voltage dip at PCC is supposed and DFIG parameters are listed in Table 1. It can be seen in Fig. 9 that the stator and rotor currents are within prescribed limits of overcurrent. The selection of crowbar resistance, according to method-2, considers the maximum rotor voltage together with rotor overcurrent limits. So, the converter damage possibility due to overvoltage and overcurrent is much smaller than that in method-1. In this point, it can be concluded that the method-2 is better than the method-1.

B. IMPACT OF GRID IMPEDANCE

Installation of new wind farms to the existing grid is continuously increasing. As a consequence, the overall grid impedance in the future grid would decrease. Fig. 10 shows the schematic diagram of multiple wind farm connected to

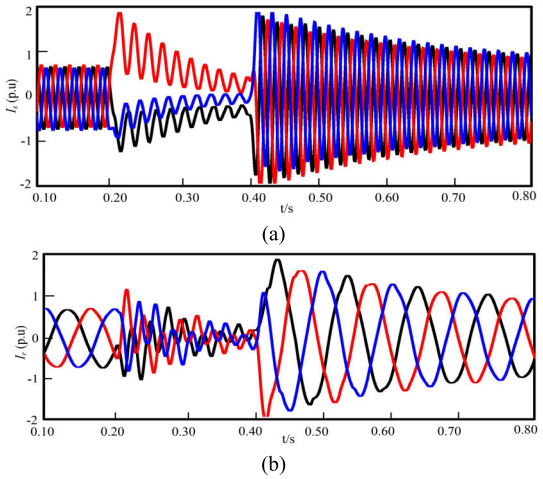

FIGURE 9. Simulation results of method-2 under 90% voltage dip. (a) Stator current of DFIG (method-2); (b) Rotor current of DFIG (method-2).

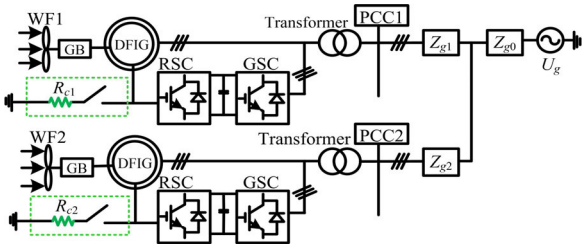

FIGURE 10. Multiple wind farms connected to the grid.

the power grid. When wind farm 1 is connected to the grid, the grid impedance is $Z_1 = Z_{g1} + Z_{g0}$. Connecting the wind farm 2 to the grid together with the present WF1, the equivalent grid impedance (Z_2) is reduced to $Z_2 = Z_{g1} + Z_{g0} \| Z_{g2}$. It shows the impact of the grid impedance to the DFIG would be small if the grid is very strong, where Z_{g0} could be neglected at the strong ideal grid and then impedance Z_1 is unchangeable.

For practical distribution power grid, the grid impedance is proportional to the short circuit capacity. The short circuit capacity is normally increased with the increasing grid strength, where more wind farms are connected to the grid, the more will be the grid strength. Supposing $|Z_1| = 2.18\Omega$, and $|Z_2| = 0.7\Omega$ to reflect the above two cases of the present grid (16 kA) and future grid (50 kA) with more power sources, the stator and rotor currents with traditional rotor crowbar (method-1 and method-2) for the grid-connected DFIG is shown in Fig. 11 and Fig. 12, respectively. Here the current of the DFIG connected with PCC1 is observed to evaluate the performance of the rotor crowbar. In both cases, the rotor crowbar resistance is selected according to (20), which is not related to the grid impedance.

It can be seen in Fig. 11(a) that stator current is below 2 p.u. if the DFIG is connected to the grid with present grid impedance. However, the stator current will cross the limit of

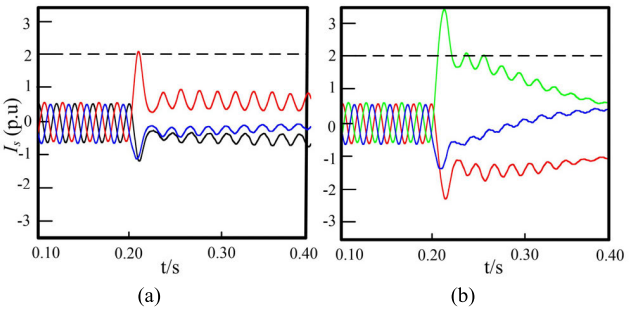

FIGURE 11. Stator current of DFIG. (a) Case 1, (b) Case 2.

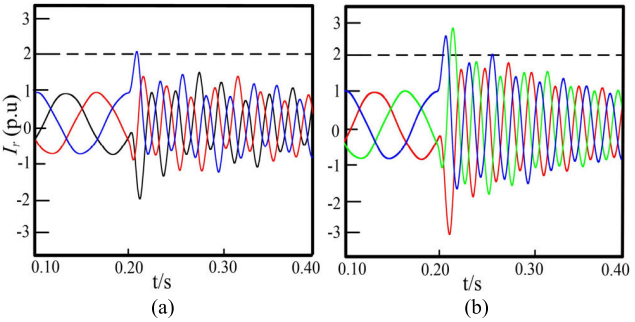

FIGURE 12. Rotor current of DFIG. (a) Case 1, (b) Case 2.

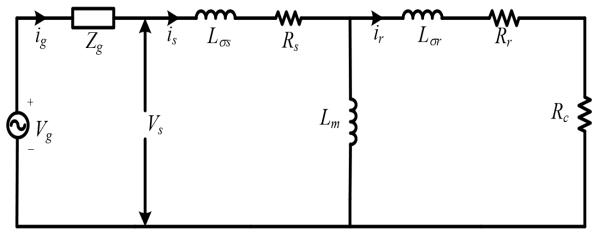

FIGURE 13. Schematic diagram for DFIG with grid parameters.

overcurrent even though the crowbar is in action in the future grid impedance, as shown in Fig. 11(b).

Likewise, the rotor current with different grid impedance can be seen in Fig. 12.

From the aforementioned analysis, it can be concluded that large interference of grid impedance will cause the occurrence of overcurrent, which means the failure of the rotor crowbar technique. So the design rules of the crowbar resistance need to be reconstructed by taking the grid impedance into consideration.

C. MODIFICATIONS OF CROWBAR RESISTANCE

The grid impedance is in series with the stator of DFIG, decreasing the grid impedance will increase the stator and rotor current of DFIG under fault condition and hence degrades the DFIG performance under LVRT.

The schematic diagram of grid-connected DFIG with DFIG considering the grid impedance is shown in Fig. 13.

Where V_g and V_s are grid voltage and PCC voltage, respectively. Z_g is the Thevenin equivalent impedance of the grid,

transmission line, and transformers. Considering the grid impedance Z_g, the stator voltage V_s of the DFIG is given by

$$V_s = V_g + i_s Z_g \tag{22}$$

where V_g is the grid voltage and i_s is the stator current of DFIG.

Substituting (22) into (1), it yields

$$V_s = \left(R_s + Z_g\right) i_s + \frac{d\psi_s}{dt} + j\omega_s \psi_s \tag{23}$$

Similarly, considering the grid impedance, the stator flux can be given by

$$\vec{\psi}_s = \frac{(1-d)U_{sN}}{j\omega_s} + \frac{dU_{sN}}{j\omega_s} e^{-\frac{t}{\tau_{s1}}} \tag{24}$$

$$\tau_{s1} = \frac{L_s}{R_s + Z_g} \tag{25}$$

Considering the grid impedance, (18) can be re-written as

$$\begin{aligned}\vec{e}_r = {} & \frac{L_m}{L_s} s(1-d) U_{sN} e^{js\omega_s t} \\ & - \frac{L_m}{L_s} d(1-s) \frac{U_{sN}}{j\omega_s} \left(\frac{R_s + Z_g}{L_s}\right) e^{-t(R_s+Z_g)/L_s} \\ & + j\omega_r \frac{L_m}{L_s} d(1-s) \frac{U_{sN}}{j\omega_s} e^{-t(R_s+Z_g)/L_s}\end{aligned} \tag{26}$$

Using Euler identity, (26) can be rewritten as

$$\begin{aligned}\vec{e}_r = {} & (1-d)s\cos(s\omega_s t) - \frac{d\omega_r}{\omega_s} e^{-t(R_s+Z_g)/L_s} \\ & + j(1-d)_S \sin(s\omega_s t) + \left(\frac{R_s+Z_g}{L_s\omega_s}\right) de^{-t(R_s+Z_g)/L_s}\end{aligned} \tag{27}$$

During crowbar action with blocked RSC, the DFIG impedance is given as

$$Z_{DFIG} = R_{DFIG} + jX_{DFIG} \tag{28}$$

where the resistance and reactance of DFIG is given by [37]

$$R_{DFIG} = R_s + \frac{(R_r + R_c/s)X_m^2}{(R_r + R_c/s)^2 + (X_m + X_r)^2} \tag{29a}$$

$$X_{DFIG} = X_s + \frac{X_m\left((R_r + R_c/s)^2 + X_r(X_m + X_r)\right)}{(R_r + R_c/s)^2 + (X_m + X_r)^2} \tag{29b}$$

The fault current analysis of the DFIG system without a crowbar and the grid impedance has been studied in details in [38]. According to Fig. 13, the stator transient current can be expressed as

$$i_s(t) = \frac{Z_s\left(V_g - \frac{j\omega_s L_m (R_s + j\omega_s\sigma L_s) V_r}{j\omega_s(1-\sigma)(R_r+R_c)L_s}\right)}{\left(1 - Z_s Z_g e^{-\left(\frac{1}{\tau_{AC}} + j\omega_{AC}\right)t}\right)} e^{-\left(\frac{1}{\tau_{AC}} + j\omega_{AC}\right)t} \tag{30}$$

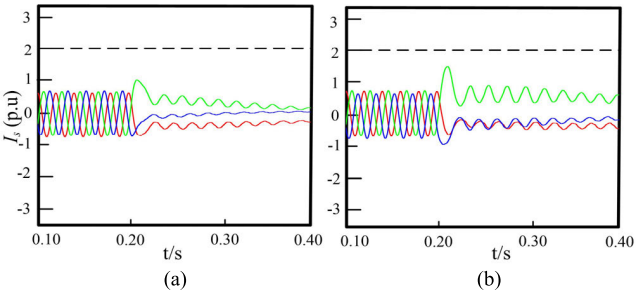

FIGURE 14. Stator current of DFIG with modified method. (a) Case 1, (b) Case 2.

In (30), Z_s, and the time constant can be expressed as

$$Z_s = \frac{(R_r + R_c)\left(1 - \frac{(R_s + j\omega_s L_s)}{(R_s + j\omega_s\sigma L_s)}\right)}{(R_r + R_c)(R_s + j\omega_s L_s) + j(\omega_s - \omega_r) L_r (R_s + j\omega_s\sigma L_s)} \tag{31}$$

$$i\frac{1}{\tau_{AC}} + j\omega_{AC} \approx \frac{(R_r + R_c)(R_s + j\omega_s L_s)}{L_r (R_s + j\omega_s\sigma L_s)} - j\omega_r \tag{32}$$

The voltage across the crowbar resistor and hence the voltage across the rotor and RSC can be expressed as

$$\sqrt{2} V_{r\max} \approx R_c i_{r\max} \tag{33}$$

Combing (30) and (33) with the assumptions that maximum amplitude of the stator and rotor currents are approximately equaled, the maximum value of R_c can be expressed as (34), as shown at the bottom of this page, where A, B, C, D, F and G in (34) are given as

$$\begin{cases} A = \left(1 - \dfrac{R_s + j\omega_s L_s}{R_s + j\sigma\omega_s L_s}\right) \\ B = R_s + j\omega_s L_s \\ C = j(\omega_s - \omega_r) L_r (R_s + j\sigma\omega_s L_s) \\ D = j\omega_s L_s V_{r\max} (R_s + j\sigma\omega_s L_s) \\ F = j\omega_s (1-\sigma)(R_r + R_s) L_s \\ G = \sqrt{2} V_{r\max} \end{cases} \tag{35}$$

Based on (34) and (35), with the grid impedance $|Z_1| = 2.18\Omega$, the calculated value of R_c comes out to be 2.5Ω.

Supposing two cases of different grid impedance similar to method-1 and method-2 with $|Z_1| = 2.18\Omega$, and $|Z_2| = 0.7\Omega$. The stator and rotor currents with a modified crowbar ($R_c = 2.5\Omega$) for multiple grids connected DFIG is shown in Fig. 14 and Fig. 15, respectively. It can be seen in Fig. 14 that under both case the stator current is below the limit of overcurrent. Similarly, it can be seen in Fig. 15 that the rotor current under different grid impedance is below the limit of overcurrent.

The aforementioned discussions verify the analytical expression of R_c. Moreover, it can be concluded that R_c taking

$$R_c = \left| -\left(AV_g R_r - GB - AGZ_g + {}^{AD}/_{F}\right) \pm \sqrt{\left(AV_g R_r - GB - AGZ_g + {}^{AD}/_{F}\right)^2 + 4AV_g R_r \left(GB + AGZ_g\right)} \Big/ 2AV_g \right| \tag{34}$$

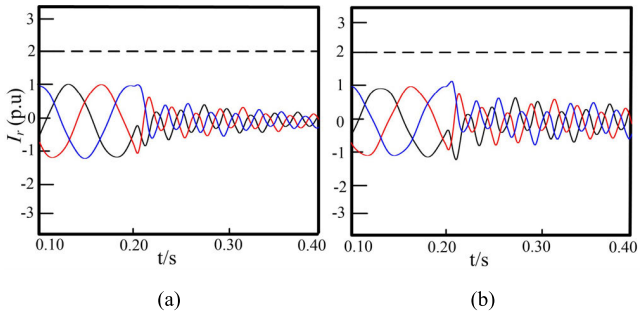

FIGURE 15. Rotor current of DFIG with modified method. (a) Case 1, (b) Case 2.

TABLE 2. Crowbar resistance for different methods.

Method	Crowbar resistance (Ω)
Method-1	0.59
Method-2	0.61
Modified method	2.5

the grid impedance into considerations keeps the stator and rotor current well below the overcurrent limits.

D. DISCUSSIONS

The value of R_c is an important parameter of grid-connected DFIG system to limit the rotor current and the rotor voltage during grid faults. The crowbar resistance R_c might be calculated by the different methods and the value of R_c is shown in Table 2 under the parameters of Table 1. In Table 2, the value of R_c according to modify method is higher than the other three methods because in the modified method the impact of the grid impedance is considered.

The stator currents under 90% grid voltage dip are simulated with the crowbar resistance selected by different methods, and the simulation results are given in Fig. 16, where the amplitude of the stator current is plotted against time. The red, blue and black curve represents the traditional methods, i.e., the crowbar resistance without grid impedance, while the modified method is shown with the pink color. Before the time of 0.62 seconds, the system is supposed in a normal state, and the stator current has the same value. However, the peak value of stator current according to the modified method is lower than the traditional methods after the grid low voltage fault occurs. It can be seen from Fig. 16 that there are fewer oscillations and fast recovery of rotor and stator post-fault transient current may be achieved for the crowbar resistance of modifying method. So considering the grid parameters in R_c calculation, the stator short-circuits current is decreased, which may enhance the lifespan of the wind turbines.

The index for LVRT is defined to show the impact of grid impedance on the crowbar resistance and compare the LVRT performance of the DFIG with different crowbar resistance and can be expressed as

$$LV_I = \int \left(a_1 \left|I_{r,\max} - I_{r,ref}\right| + a_2 \left|I_{s,\max} - I_{s,ref}\right|\right) dt \quad (36)$$

where LV_I is the LVRT index, $I_{r,max}$, and $I_{r,ref}$ is the maximum and reference rotor current, respectively.

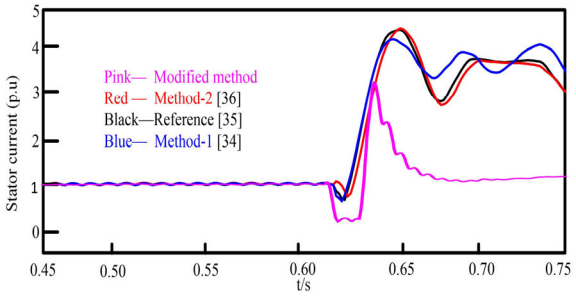

FIGURE 16. Comparisons of stator current for different methods.

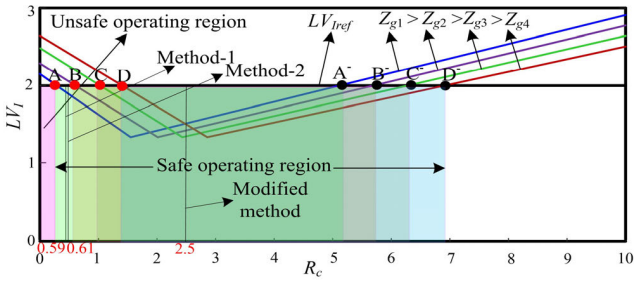

FIGURE 17. LVRT Index vs crowbar resistance with different grid impedance.

Similarly, $I_{s,max}$, and $I_{s,ref}$ is the maximum and reference stator current, respectively. a_1 and a_2 are the weight of the rotor and stator current, respectively.

The LVRT index can be found from (36) and plotted against the crowbar resistance, as shown in Fig. 17. The LVRT index will intersect the threshold value at two points. The distance between the two intersection points is called a safe space. The region to the left of the first intersection point is called unsafe space. So the LVRT index for different grid impedance corresponds to different space. To check whether the crowbar resistance selected by traditional and modified method lies in the safe or unsafe space, different grid impedance Z_{g1}, Z_{g2}, Z_{g3}, and Z_{g4} is adopted as 2.18Ω, 0.7Ω, 0.53Ω and 0.43 Ω, respectively. The LVRT index depends on the grid impedance as can be seen in Fig. 17. For set LVRT index, the safe space might be obtained by the distance of the intersection points. Such as, for grid impedance Z_{g1}, the safe space is AA^- and for grid impedance Z_{g2}, the safe space is BB^-. Similarly, grid impedance Z_{g3} corresponds to the safe space CC^-, while the safe space is DD^- for grid impedance Z_{g4}. The crowbar resistance selected by method-1 and method-2 may realize LVRT at certain grid impedance; however, it still has the risk for operating out of the safe space when the grid impedance decreases greatly. For the modified method proposed in this paper, the selected crowbar resistance moves right side and much more fits for the safe space. So, in this case, the rotor crowbar technique will be robust to the grid impedance.

From the aforementioned discussions, it can be concluded that the grid impedance does impact on the selection of crowbar resistance. It shows crowbar resistance selected by the modified method is optimal than others.

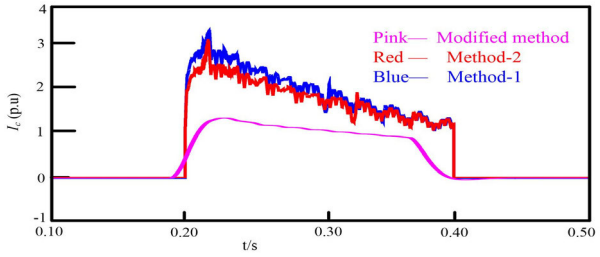

FIGURE 18. Comparisons of crowbar current for different methods.

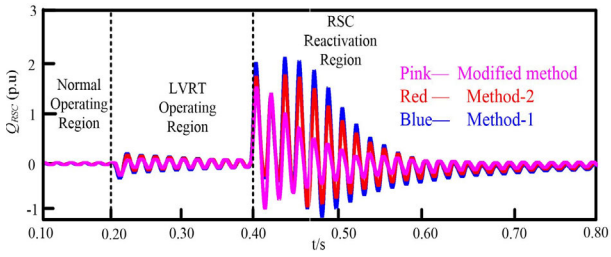

FIGURE 19. Comparisons of reactive power output of RSC for different methods.

The crowbar current for different resistance selection methods taking the grid impedance into consideration with 90% voltage dip at the grid from 0.2 to 0.4 seconds is shown in Fig. 18. It can be seen in Fig. 18 that the amplitude of the crowbar current using the traditional method of crowbar resistance selection (method-1 and method-2) is higher than the modified method. Furthermore, it can be seen that there are fewer oscillations in the crowbar current by using the modified method. So crowbar resistance selected by modified method may enhance the lifespan of the rotor crowbar.

The reactive power output of the RSC for different resistance selection methods taking the grid impedance into consideration with 90% voltage dip at the grid from 0.2 to 0.4 seconds is shown in Fig. 19.

There are three regions in Fig. 19. In the normal operating region the reactive power of the RSC is zero. In the LVRT operating region, the RSC is blocked, and there can be seen a fewer oscillation. However, after the crowbar is deactivated, the RSC reactivates, which causes large oscillations in the reactive power as can be seen in Fig. 19. Additionally, it can be seen in Fig. 19 that the reactive power output of RSC using the traditional method of crowbar resistance selection (method-1 and method-2) in the RSC reactivation region is higher than the modified method. The crowbar cannot provide reactive power to the grid during fault events, and it is the major disadvantage of crowbar technology.

V. CONCLUSION

Improvements in LVRT performance of DFIG system with rotor crowbar considering the grid impedance is studied in this paper. The index for LVRT is developed based on stator and rotor current under grid voltage dips. Additionally, the analytical expression for the crowbar resistance considering the grid impedance is derived. It has been shown that grid impedance does impact on the crowbar resistance and crowbar resistance selected by the traditional method is close to the edge of the safe space on LVRT. While the crowbar resistance shown in the modified method fits the safe space better by taking the grid impedance into considerations, and it is prevailing to the other traditional crowbar selection methods.

REFERENCES

[1] I. Erlich and U. Bachmann, "Grid code requirements concerning connection and operation of wind turbines in Germany," in *Proc. IEEE Power Eng. Soc. Gen. Meeting*, Jun. 2005, pp. 1253–1257.

[2] V. F. Mendes, C. V. de Sousa, W. Hofmann, and S. R. Silva, "Doubly-fed induction generator ride-through fault capability using resonant controllers for asymmetrical voltage sags," *IET Renew. Power Gener.*, vol. 9, no. 7, pp. 783–791, 2015.

[3] F. Poitiers, T. Bouaouiche, and M. Machmoum, "Advanced control of a doubly-fed induction generator for wind energy conversion," *Electr. Power Syst. Res.*, vol. 79, no. 7, pp. 1085–1096, 2009.

[4] B. H. Chowdhury and S. Chellapilla, "Double-fed induction generator control for variable speed wind power generation," *Electr. Power Syst. Res.*, vol. 76, nos. 9–10, pp. 786–800, 2006.

[5] O. E. Elbashir, Z. Wang, and Q. Liu, "Modeling and analysis of DFIG in wind energy conversion system," *Int. J. Energy Environ.*, vol. 5, no. 2, pp. 239–250, 2014.

[6] L. Xiong, J. Zhang, C. Wu, and M. Cheng, "Low voltage ride through device for wind turbines with series coupled compensation converter," in *Proc. Int. Conf. Elect. Mach. Syst.*, Oct. 2014, pp. 372–377.

[7] Z. Din, J. Zhang, J. Zhao, and Y. Jiang, "Doubly fed induction generator with cascade converter for improving dynamic performances," in *Proc. IEEE Energy Convers. Congr. Expo. (ECCE)*, Sep. 2018, pp. 2568–2575.

[8] J. Morren and S. W. H. de Haan, "Ridethrough of wind turbines with doubly-fed induction generator during a voltage dip," *IEEE Trans. Energy Convers.*, vol. 20, no. 2, pp. 435–441, Jun. 2005.

[9] J. Niiranen, "Voltage dip ride through of a doubly-fed generator equipped with an active crowbar," in *Proc. Nordika Wind Power Conf.*, Mar. 2004, pp. 1–4.

[10] A. Dittrich and A. Stoev, "Comparison of fault ride-through strategies for wind turbines with DFIM generators," in *Proc. Eur. Conf. Power Electron. Appl.*, Sep. 2005, pp. 1–4.

[11] V. Akhmatov, *Induction Generators for Wind Power*. Brentwood, LA, USA: Multi-Science, 2005.

[12] A. H. Kasem, E. F. El-Saadany, H. H. El-Tamaly, and M. A. A. Wahab, "An improved fault ride-through strategy for doubly fed induction generator-based wind turbines," *IET Renew. Power Gener.*, vol. 2, no. 4, pp. 201–214, Dec. 2008.

[13] S. Foster, L. Xu, and B. Fox, "Coordinated reactive power control for facilitating fault ride through of doubly fed induction generator- and fixed speed induction generator-based wind farms," *IET Renew. Power Gener.*, vol. 4, no. 2, pp. 128–138, 2010.

[14] L. Peng, B. Francois, and Y. Li, "Improved crowbar control strategy of DFIG based wind turbines for grid fault ride-through," in *Proc. IEEE Appl. Power Electron. Conf. Expo. (APEC)*, Feb. 2009, pp. 1932–1938.

[15] M. B. C. Salles, J. R. Cardoso, A. P. Grilo, C. Rahmann, and K. Hameyer, "Control strategies of doubly fed induction generators to support grid voltage," in *Proc. IEEE Int. Electr. Mach. Drives Conf.*, May 2009, pp. 1551–1556.

[16] J. López, E. Gubía, E. Olea, J. Ruiz, and L. Marroyo, "Ride through of wind turbines with doubly fed induction generator under symmetrical voltage dips," *IEEE Trans. Ind. Electron.*, vol. 56, no. 10, pp. 4246–4254, Oct. 2009.

[17] L. G. Meegahapola, T. Littler, and D. Flynn, "Decoupled-DFIG fault ride-through strategy for enhanced stability performance during grid faults," *IEEE Trans. Sustain. Energy*, vol. 1, no. 3, pp. 152–162, Jul. 2010.

[18] M. Q. Duong, G. N. Sava, F. Grimaccia, S. Leva, M. Mussetta, S. Costinas, and N. Golovanov, "Improved LVRT based on coordination control of active crowbar and reactive power for doubly fed induction generators," in *Proc. 9th Int. Symp. Adv. Topics Elect. Eng. (ATEE)*, May 2015, pp. 650–655.

[19] M. Mohseni, S. M. Islam, and M. A. S. Masoum, "Enhanced hysteresis-based current regulators in vector control of DFIG wind turbines," *IEEE Trans. Power Electron.*, vol. 26, no. 1, pp. 223–234, Jul. 2011.
[20] J. Liang, D. F. Howard, J. A. Restrepo, and R. G. Harley, "Feedforward transient compensation control for DFIG wind turbines during both balanced and unbalanced grid disturbances," *IEEE Trans. Ind. Appl.*, vol. 49, no. 3, pp. 1452–1463, May 2013.
[21] M. Rahimi and M. Parniani, "Transient performance improvement of wind turbines with doubly fed induction generators using nonlinear control strategy," *IEEE Trans. Energy Convers.*, vol. 25, no. 2, pp. 514–525, Oct. 2009.
[22] S. Q. Bu, W. Du, H. F. Wang, and S. Gao, "Power angle control of grid-connected doubly fed induction generator wind turbines for fault ride-through," *IET Renew. Power Gener.*, vol. 7, pp. 18–27, Jan. 2013.
[23] Z. Song, T. Shi, C. Xia, and W. Chen, "A novel adaptive control scheme for dynamic performance improvement of DFIG-based wind turbines," *Energy*, vol. 38, no. 1, pp. 104–117, 2012.
[24] M. Q. Duong, F. Grimaccia, S. Leva, M. Mussetta, and K. H. Le, "A hybrid fuzzy-PI cascade controller for transient stability improvement in DFIG wind generators," in *Proc. IEEE Int. Conf. Fuzzy Syst. (FUZZ-IEEE)*, Jul. 2016, pp. 1733–1739.
[25] M. Q. Duong and G. N. Sava, "Coordinated reactive power control of DFIG to improve LVRT characteristics of FSIG in wind turbine generation," in *Proc. 11th Int. Conf. Electromech. Power Syst. (SIELMEN)*, Jan. 2017, pp. 256–260.
[26] D. Zhu, X. Zou, L. Deng, Q. Huang, S. Zhou, and Y. Kang, "Inductance-emulating control for DFIG-based wind turbine to ride-through grid faults," *IEEE Trans. Power Electron.*, vol. 32, no. 11, pp. 8514–8525, Nov. 2017.
[27] J. Chen, Y. Wang, M. Zhu, Q. Yu, and J. Li, "Improved rotor braking protection circuit and self-adaptive control for DFIG during grid fault," *Energies*, vol. 12, no. 10, p. 1994, 2019.
[28] A. El-Naggar and I. Erlich, "Short-circuit current reduction techniques of the doubly-fed induction generator based wind turbines for fault ride through enhancement," *IET Renew. Power Gener.*, vol. 11, no. 7, pp. 1033–1040, 2017.
[29] A. D. Hansen, P. Sørensen, F. Iov, and F. Blaabjerg, "Control of variable speed wind turbines with doubly-fed induction generators," *Wind Eng.*, vol. 28, no. 4, pp. 411–432, 2004.
[30] G. Abad, J. Lopez, M. A. Rodriguez, L. Marroyo, and G. Iwanski, *Doubly Fed Induction Machine: Modeling and Control for Wind Energy Generation*. Hoboken, NJ, USA: Wiley, 2011.
[31] R. A. J. Amalorpavaraj, P. Kaliannan, S. Padmanaban, U. Subramaniam, and V. K. Ramachandaramurthy, "Improved fault ride through capability in DFIG based wind turbines using dynamic voltage restorer with combined feed-forward and feed-back control," *IEEE Access*, vol. 5, pp. 20494–20503, 2017.
[32] R. Pena, J. C. Clare, and G. M. Asher, "Doubly fed induction generator using back-to-back PWM converters and its application to variable-speed wind-energy generation," *IEE Proc.-Electr. Power Appl.*, vol. 143, no. 3, pp. 231–241, 1996.
[33] J. Lopez, P. Sanchis, X. Roboam, and L. Marroyo, "Dynamic behavior of the doubly fed induction generator during three-phase voltage dips," *IEEE Trans. Energy Convers.*, vol. 22, no. 3, pp. 709–717, Sep. 2007.
[34] M. Wang, W. Xu, H. Jia, and X. Yu, "A novel method to optimize the active crowbar resistance for low voltage ride through operation of doubly-fed induction generator based on wind energy," in *Proc. IEEE Int. Symp. Ind. Electron.*, May 2012, pp. 957–962.
[35] J. Morren and S. W. H. D. Haan, "Short-circuit current of wind turbines with doubly fed induction generator," *IEEE Trans. Energy Convers.*, vol. 22, no. 1, pp. 174–180, Mar. 2007.
[36] X. Zhang, Q. Li, S. Yang, Z. Xie, and R. Cao, "Response and protection of DFIG system under grid fault," in *Proc. Asia–Pacific Power Energy Eng. Conf.*, Mar. 2010, pp. 1–5.
[37] W. Zhang, H. Ma, J. Zhang, L. Chen, and Y. Qu, "Multi-objective fuzzy-optimization of crowbar resistances for the low-voltage ride-through of doubly fed induction wind turbine generation systems," *J. Power Electron.*, vol. 15, no. 4, pp. 1119–1130, 2015.
[38] A. El-Naggar, "Advanced modeling and analysis of the doubly-fed induction generator based wind turbines," Ph.D. dissertation, Univ. Duisburg-Essen, Duisburg, Germany, 2017.

ZAKIUD DIN received the B.Sc. degree in electrical engineering with major in electrical power system and the M.Sc. degree in electrical engineering from the University of Engineering and Technology, Peshawar, Pakistan, in 2008 and 2013, respectively. He is currently pursuing the Ph.D. degree with the School of Electrical Engineering, Southeast University, Nanjing, China. From 2010 to 2016, he served for the Sarhad University of Science and Information Technology, Peshawar, as a Lecturer. His current research interests include wind power generation system and power electronics.

JIANZHONG ZHANG (M'08–SM'16) received the M.Sc. and Ph.D. degrees in electrical engineering from the Department of Electrical Engineering, Southeast University, Nanjing, China, in 2005 and 2008, respectively.

From 2006 to 2007, he was a Visiting Scholar with the Department of Energy Technology, Aalborg University, Aalborg, Denmark. Since 2008, he has been with Southeast University, where he is currently a Research Professor with the School of Electrical Engineering. He was a Visiting Professor with the Worcester Polytechnic Institute, Worcester, USA, in July 2012. His research interests include electric machines, power electronics, and wind power generation. Dr. Zhang was a recipient of the Institution Premium Award of the Institutions of Engineering and Technology, U.K.

YAODONG ZHU received the M.Sc. and Ph.D. degrees in test measurement technology and instrument from the Department of Automation, Nanjing University of Aeronautics and Astronautics, Nanjing, China, in 2000 and 2003, respectively.

Since 2005, he has been with Jiaxing University, where he is currently an Associate Professor with the School of Mechanical and Electrical Engineering. His research interests include smart robot, embedded computing, and computer vision.

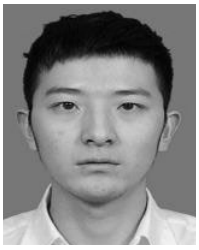

ZHENG XU received the B.Sc. degree in wind energy and power engineering from Hohai University, Nanjing, China, in 2013, and the M.Sc. degree in electrical engineering from Tongji University, Shanghai, China, in 2016. He is currently pursuing the Ph.D. degree with the Department of Electrical Engineering, Southeast University, Nanjing.

His research interests include electric machine design and fault diagnosis.

AHMED EL-NAGGAR (SM'12) was born in Alexandria, Egypt, in 1984. He received the B.Sc. in electrical power and machines from the University of Alexandria, Egypt, the M.Sc. degree from Brandenburg Technical University (BTU), Cottbus, Germany, in 2012, and the Ph.D. degree from the University of Duisburg-Essen, in 2017.

From 2008 to 2009, he was an Electrical Design Engineer with SEG Middle-East Abu Dhabi, United Arab Emirates (UAE). He is currently a Senior Power System Consultant with GE Energy Consulting. His major research interests include power system stability and control, modeling, and simulation of power system dynamics, including intelligent system applications.